Sánchez Tovar, R.; Lee, K.; Garcia-Anton, J.; Schmuki, P. (2013). Photoelectrochemical Properties of Anodic TiO2 Nanosponge Layers. ECS Electrochemistry Letters. 2(3):9-11. doi:10.1149/2.005303eel.

# Photoelectrochemical properties of anodic $TiO_2$ nanosponge layers

Rita Sánchez-Tovar[1,2], Kiyoung Lee[1], Jose García-Antón[2], Patrik Schmuki[1]*

[1]Department of Materials Science and Engineering, WW4-LKO, University of Erlangen-Nuremberg, Martensstrasse 7, D-91058 Erlangen, Germany

[2] Ingeniería Electroquímica y Corrosión, Departamento de Ingeniería Química y Nuclear, Universitat Politècnica de València, Camino de Vera s/n, 46022 Valencia, Spain

## Abstract

In the present work we grow $TiO_2$ nanosponge structures by anodizing Ti in a glycerol/water/$NH_4F$ electrolyte to thickness of some μm. We evaluate the photoelectrochemical behavior (band gap, photocurrent-voltage characteristics) in presence and absence of methanol. Methanol drastically affects the photoresponse (due to hole capture and current doubling). The optimum thickness for photoelectrochemical applications of these nanostructures is dependent on the excitation wavelength. For applications such as solar light water splitting, anodic sponge structure of ≈ 500 nm thickness can be beneficially used to increase the photoresponse compared to compact $TiO_2$ layers.

*Keywords:* $TiO_2$, self-organization, porous structure, anodization.

* Corresponding author: Tel.: +49-9131-852-7575, Fax.: +49-9131-852-7582

E-mail: schmuki@ww.uni-erlangen.de

## 1. Introduction

$TiO_2$ is probably the most studied oxide in materials science. This is due to the many functional properties of this oxide that enable for example its application in photocatalysis [1-3], solar cells [4], self-cleaning devices [5, 6], and for bio medical materials [7, 8]. Frequently, $TiO_2$ is used in the nanoparticle form to establish a high surface area [9, 10], for example for photoelectrodes in photoelectrochemical applications [11]. Nevertheless, such particles need to be compacted or sintered onto a back contact to establish a functional photoelectrode. Therefore, oxide layers formed by anodization on a metallic substrate possess the inherent advantage that they are directly back-contacted. In order to obtain high surface area structures, various self-organizing anodic oxidation pathways have been explored. Over the past 10 years not only $TiO_2$ nanotubes have been widely examined [12] but also "non-thickness limited" ordered channel layers attracted wide interest [13]. Most recently [14], another morphology, anodic nanosponge layers, were observed when using anodization with a rotating electrode configuration.

This nanosponge structure, which consists of a strongly interlinked network of $TiO_2$, offers a considerably higher specific surface area than $TiO_2$ nanotubes and provides, at the same time, a directly connected path for electrons (in contrast to compacted nanoparticles).

In the present work, we investigate the photoelectrochemical properties of this nanosponge morphology.

## 2. Experimental

Nanosponge layers were formed to thickness varying from 0.5 - 4 μm. 0.5 μm and 1μm thick layers were obtained by anodization of titanium foils (99.6%, 0.1 mm thick, Advent Research Materials Ltd.) and were in a Glycerol:$H_2O$ 60:40 vol.% + 0.27 M $NH_4F$ electrolyte (using a voltage ramp of 0.2 $Vs^{-1}$) and a final potential at 60 V with a holding time of 0 min and 30 min, respectively. 2 and 4 μm thick nanosponges were grown by anodization of Ti rods at 30 V (0.2 $Vs^{-1}$) during 3 hr in Glycerol:$H_2O$ 50:50 vol.% and 60:40 vol.% + 0.27 M $NH_4F$ electrolyte and using for the latter a rotation speed of 200 $rads^{-1}$. For compact $TiO_2$ layer the Ti foils anodized as previously described [15] in 1M $H_2SO_4$ at 20 V during 20 min.

A field-emission scanning electron microscope (Hitachi FE-SEM S4800) was used for morphological characterization. X-ray diffraction analysis (XRD) was performed with a Philips X'pert MPD with a Panalytical X'celerator detector using graphite-monochromatized Cu Kα radiation. XPS measurements were carried out by X-ray photoelectron spectroscopy (PHI 5600, Physical Electronics) using Al Kα monochromatized radiation.

Photoelectrochemical studies and water splitting measurements were carried out using as-formed $TiO_2$ nanosponges and corresponding samples annealed in a furnace at 450 °C in air for 1 h. The photocurrent measurements were carried out as described previously in a 0.1 M $Na_2SO_4$ and in 0.1 M $Na_2SO_4$ + 2 M methanol electrolytes.

Photoelectrochemical water splitting experiments were carried out under simulated sunlight condition AM 1.5 (100 mW/cm²) in 1 M KOH solution as described in Ref [16].

## 3. Results and discussion

Figure 1 shows scanning electron microscope (SEM) images of $TiO_2$ nanosponges grown to different thicknesses from 0.5 to 4 μm (the images show both cross-sections and top-surfaces). From the images it is evident that the typical feature size of the $TiO_2$ scaffold is in the range of 50-100 nm and the pore openings are in the range of 50 to 85 nm.

X-ray diffraction (XRD) measurements (see example in Figure 2a) show that the as-prepared $TiO_2$ nanosponge layers are amorphous. Annealing in air at 450 ºC during 1 hour was carried out to crystallize the material to anatase. The XRD results confirm successful conversion, and the evaluation of the main anatase (101) peak of $25.2^o$ in terms of the Scherrer equation yields an average crystal size of ≈17 nm.

Figure 2b and c show results from XPS and EDX for the composition of an as-formed and an annealed nanosponge. Clearly, the most important difference between before and after annealing is the contents of carbon and fluorine, which are considerably lower after annealing the sponges. The high carbon peak for the as-formed sample can be attributed remnants of glycerol which was used as an electrolyte for anodization. Evidently also fluoride which is embedded during growth is at least partially lost during annealing.

Figure 3 shows the photocurrent spectra measured in the range of 300 to 460 nm for non-annealed and annealed samples at 450 ºC at 500 mV vs. Ag/AgCl in 0.1 M $Na_2SO_4$ (figure 3 (a)) and in $Na_2SO_4$ + 2 M Methanol (figure 3 (b)). The inset of figure 3 (a) shows a plot of the photocurrent data for an indirect band-gap $((ipce \cdot hv)^{0.5}\ vs. hv)$ from which it is apparent that for all annealed structures $E_g \approx 3.15$ eV can be extracted, i.e. a value that is in line with the reported band gap of anatase $TiO_2$ [15, 17]. Evidently

annealing to anatase is critical to obtain a significant photoresponse. From the magnitude of the IPCE spectra taken for the anatase sponge in the $Na_2SO_4$ solution it is apparent that for short wavelengths the 500 nm thick sponge shows the highest photoresponse. This can be explained by the fact that for deep UV the absorption coefficient of $TiO_2$ is much higher than for longer wavelengths. As a result, deep UV is absorbed in the outermost part of the $TiO_2$ structure; the excited carriers produced by deep UV then need to travel the longest path to the back contact. In other words, the thicker the sponge layers the higher are recombination losses for deep UV [18]. For wavelengths close to the band-gap the different sponge thicknesses show a comparable photoresponse indicating that in these cases electron recombination does not depend on the layer thickness (due to the deep penetration of the structure by these excitation wavelengths). All the sponge structures show a clearly higher IPCE value over the entire spectrum than the $TiO_2$ compact layer, which confirms a superior light absorption due to the nanosponge morphology. The presence of methanol in the electrolyte drastically increases the overall IPCE value (figure 3 (b)). Methanol is reported to act as efficient hole capture agent (thus reducing surface recombination of electron-hole pairs) and/or to be an effective agent to cause current doubling effects [19]. In fact, for all the spectra of the sponge indeed a quite good agreement with a doubling of the photocurrent is observed. Figure 3 (c) and (d) show the IPCE values as a function of the potential for a wavelength of 350 nm, for $Na_2SO_4$ medium and for $Na_2SO_4$ with methanol, respectively. IPCE values increase with applied potential, reaching a steady value for the highest potentials and the thicker nanosponges (2 and 4 μm). Particularly, the behaviour of the compact surface is in line with the classic Gärtner-model [20] that predicts an $i_{ph} \propto U^{0.5}$ dependence, i.e. a photocurrent increase with the increasing

width of a Schottky type space charge layer. However, considering that for anodic annealed layers typically doping concentrations in the range of $10^{18}$-$10^{20}$ $cm^{-3}$ are reported [21], it can be expected that in the nanostructure with feature sizes in the range of 50 nm complete depletion extends over the entire structure already at a bias of a few 100 mV anodic to the flat-band potential (which can be taken as the potential of zero photocurrent in figure 3 (c) and (d)). In other words, only close to $U_{fb}$ the field can strongly contribute to carrier transport in the structure. It is thus remarkable that in the range slightly anodic to the potential of zero photocurrent, the thickest nanosponge structure shows a drastically higher photocurrent than thinner (or compact) layers.

One effect of methanol addition is that the apparent optical flat-band potential is shifted to more negative values. Therefore, it seems likely that in this potential range rapid hole capture (reducing recombination) strongly contributes to the photoresponse, while at higher potentials a current doubling seems the dominant methanol effect.

These observations are in line with the photocurrent transient measurements in figure 3e and f. At -100 mV vs. Ag/AgCl in the methanol free case the transients show a typical characteristics for an excitation-recombination process (via surface state). In the presence of methanol the recombination character becomes largely suppressed. This can be attributed to the fast hole capture in methanol. At higher potential (1 V) (figure 3g and h) the recombination character is also lost in the pure $Na_2SO_4$ electrolyte (the remaining methanol effect thus seems likely to be current doubling).

Finally, in order to assess the performance of the nanosponge excitation using the solar spectrum, samples were tested under AM1.5 (100 $mW/cm^2$) conditions (Figure 3i). The resulting photocurrent transients show the highest photocurrent density for the 500 nm thick nanosponge.

Clearly, the photocatalytic water splitting behaviour of this structure is superior to photocurrent behaviour of compact layer; nevertheless for sponge structure an optimum is reached already for comparably thin sponge layers. This illustrates that for broad-band excitation, UV contribution and thus electron transport properties dominate over surface area aspects.

## 4. Conclusions

The present work demonstrates that $TiO_2$ nanosponges can be used to generate increased photocurrent response compared with compact $TiO_2$ layers in photoelectrochemical applications. The layers show significant photocurrent amplification when methanol is added to the solution. We attribute this observation in methanol to two distinctly different effects: i) rapid hole capture that reduces surface state recombination (this effect is dominant close to $U_{fb}$), ii) current doubling (when the structure is depleted at $U \gg U_{fb}$). Moreover, the work shows that for solar applications already comparably thin sponge structures (500 nm) present the best photoelectrochemical properties.

## Acknowledgments

The authors would like to express their gratitude to the Spanish Ministry of Science and Innovation FPU grant given to Rita Sánchez Tovar, as well as DFG, and the DFG Cluster of Excellence at the University of Erlangen-Nuremberg [Engineering of Advanced Materials (EAM)] for financial support.

**References**

[1] A. Fujishima, X. Zhang, D.A. Tryk, Surf. Sci. Rep. 63, 515 (2008).

[2] M. Adachi, Y. Murata, M. Harada, Y. Yoshikawa, Chem. Lett. 29, 942 (2000).

[3] I. Paramasivam, H. Jha, N. Liu, P. Schmuki, Small 8, 3073 (2012).

[4] B. O'Regan, M. Grätzel, Nature 353, 737( 1991).

[5] A. Fujishima, K. Hashimoto, T. Watanabe, $TiO_2$ Photocatalysis: Fundamentals and Application, 1 ed. BKC, Tokyo, 1999.

[6] T. Watanabe, A. Nakajima, R. Wang, M. Minabe, S. Koizumi, A. Fujishima, K. Hashimoto, Thin Solid Films 351, 260 (1999).

[7] Y.T. Sul, C. B. Johansson, S. Petronis, A. Krozer, Y. Jeong, A. Wennerberg, T. Albrektsson, Biomaterials 23, 491 (2002).

[8] S.H. Oh, R. R. Finõnes, C. Daraio, L.H. Chen, S. Jin, Biomaterials 26, 4938 (2005).

[9] A.L. Linsebigler, G. Lu, J.T. Yates, Chem. Rev. 95, 735 (1995).

[10] M.R. Hofmann, S.T. Martin, W. Choi, D.W. Bahnemann, Chem. Rev. 95, 69 (1995).

[11] A. Hagfeldt, H. Lindström, S. Södergren, S.-E. Lindquist, J. Electroanal. Chem. 381, 39 (1995).

[12] P. Roy, S. Berger, P. Schmuki, Angew. Chem. Int. Ed. 50, 2904 (2011).

[13] K. Lee, D. Kim, P. Schmuki, Chem. Commun. 47, 5789 (2011).

[14] R. Sánchez-Tovar, K. Lee, J. García-Antón, P. Schmuki, Electrochem. Commun. 26, 1 (2013) in press.

[15] R. Beranek, H. Tsuchiya, T. Sugishima, J.M. Macak, L. Taveira, S. Fujimoto, H. Kisch, P. Schmuki Appl. Phys. Lett. 87, 243114 (2005).

[16] C. Das, P. Roy, M. Yang, H. Jha, P. Schmuki. Nanoscale 3, 3094 (2011).

[17] D. Mardare, G.I. Rusu Mater. Lett. 56, 210 (2002).

[18] R.P. Lynch, A. Ghicov, P. Schmuki, J. Electrochem. Soc. 157, G76 (2010).

[19] W.P. Gomes, T. Freund, S.R. Morrison, J. Electrochem. Soc. 115, 818 (1968).

[20] W.W. Gartner, Phys. Rev. 116, 84 (1959).

[21] J.W. Schultze, M.M. Lohrengel, Electrochim. Acta. 45, 2499 (2000).

**Figure captions**

Figure 1. Cross sectional and top surface SEM images of (a-d) $TiO_2$ nanosponge layers of different thickness and (e) compact layer.

Figure 2. (a) XRD patterns of annealed $TiO_2$ nanosponge structures of different thickness (0.5-4 μm) and of the as-formed $TiO_2$ nanosponge structure (4 μm). (b) EDX and (c) XPS spectra taken on 4 μm thick of as-formed and annealed $TiO_2$ nanosponge structures. Inset tables show detailed chemical composition. Annealing was carried out at 450 ºC for 1 h.

Figure 3. (a)-(b) IPCE spectra for different thickness (0.5-4 μm) of $TiO_2$ nanosponge structures and for the compact $TiO_2$ layer. The measurement was carried out in (a) in 0.1 M $Na_2SO_4$ and (b) 0.1 M $Na_2SO_4$ + 2 M methanol at 500 mV vs. Ag/AgCl. Inset of (a) shows band gap evaluation of $TiO_2$ nanosponges and compact layer. (c)-(d) IPCE - applied potential spectra for different thickness (0.5-4 μm) of $TiO_2$ nanosponge structures and compact layer. The measurement was carried out in (c) in 0.1 M $Na_2SO_4$ and (d) 0.1 M $Na_2SO_4$ + 2 M methanol. (e)-(h) Photocurrent transients at (e and f) -100 mV vs. Ag/AgCl and (g and h) 1 V vs. Ag/AgCl in (e and g) 0.1 M $Na_2SO_4$ and (f and h) 0.1 M $Na_2SO_4$ + 2 M methanol. (g) Photocurrent transient vs. potential curves for 0.5 to 4 μm nanosponges and compact layer in 1 M KOH solution under AM 1.5 condition.

Figure 1.

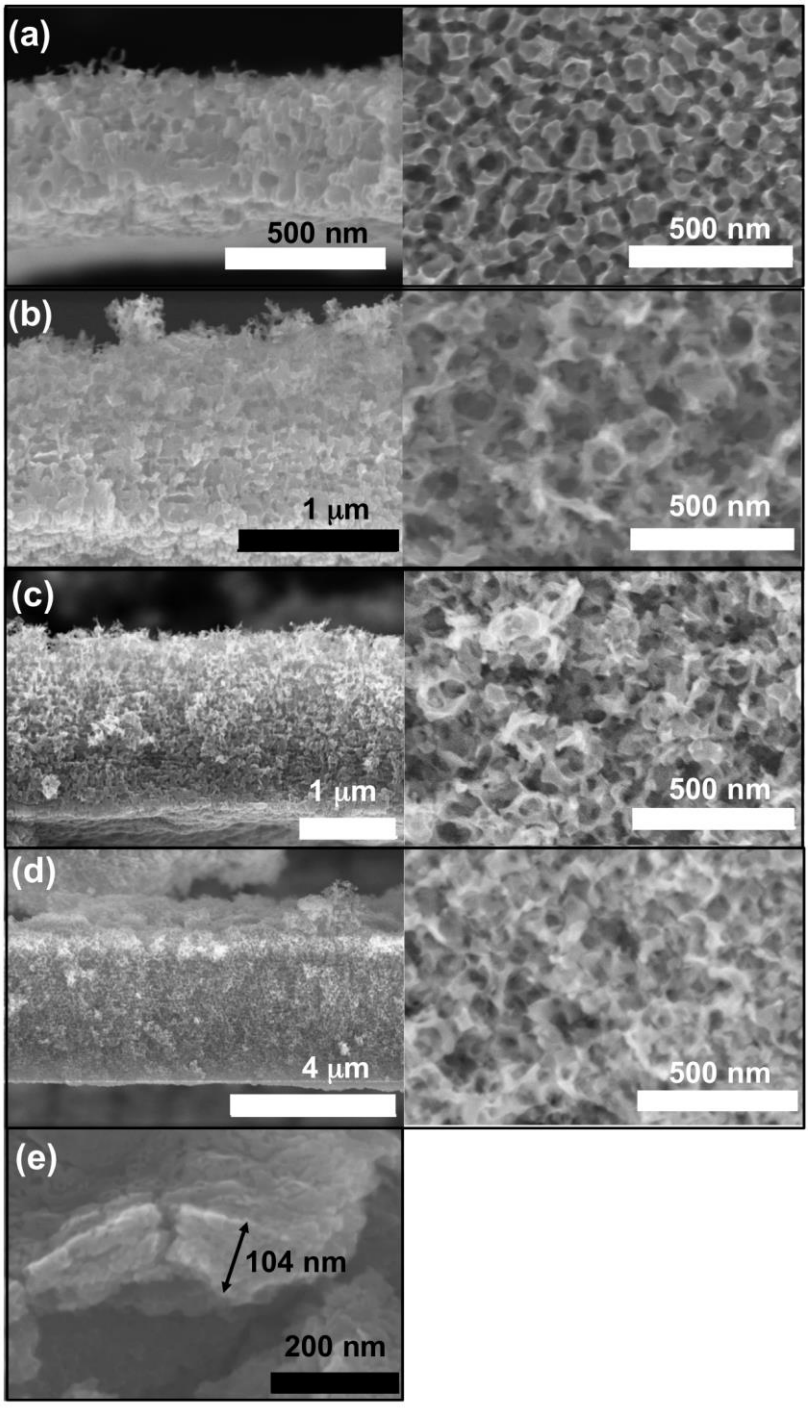

Figure 2

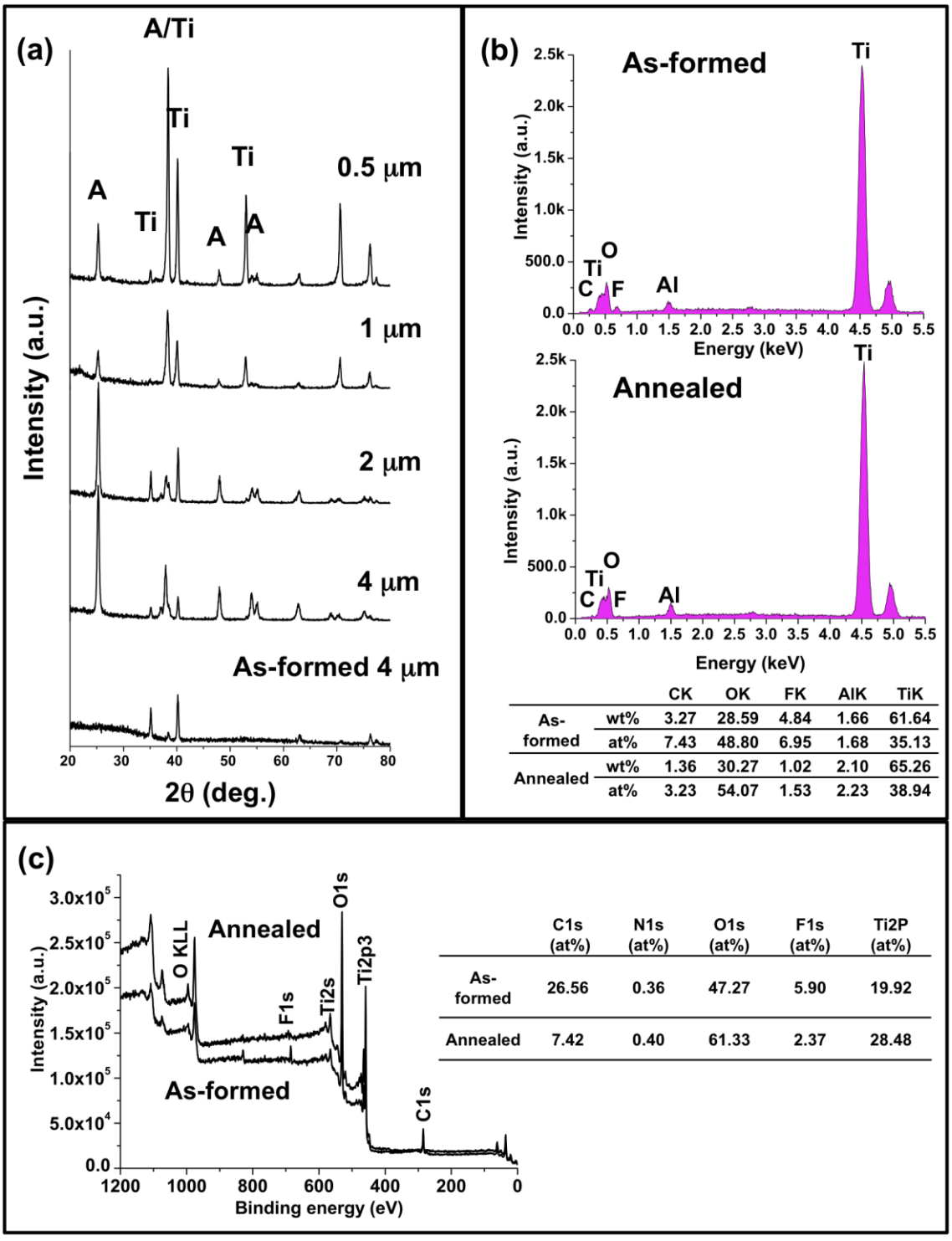


| | | CK | OK | FK | AlK | TiK |
|---|---|---|---|---|---|---|
| As-formed | wt% | 3.27 | 28.59 | 4.84 | 1.66 | 61.64 |
| | at% | 7.43 | 48.80 | 6.95 | 1.68 | 35.13 |
| Annealed | wt% | 1.36 | 30.27 | 1.02 | 2.10 | 65.26 |
| | at% | 3.23 | 54.07 | 1.53 | 2.23 | 38.94 |

| | C1s (at%) | N1s (at%) | O1s (at%) | F1s (at%) | Ti2P (at%) |
|---|---|---|---|---|---|
| As-formed | 26.56 | 0.36 | 47.27 | 5.90 | 19.92 |
| Annealed | 7.42 | 0.40 | 61.33 | 2.37 | 28.48 |

Figure 3.

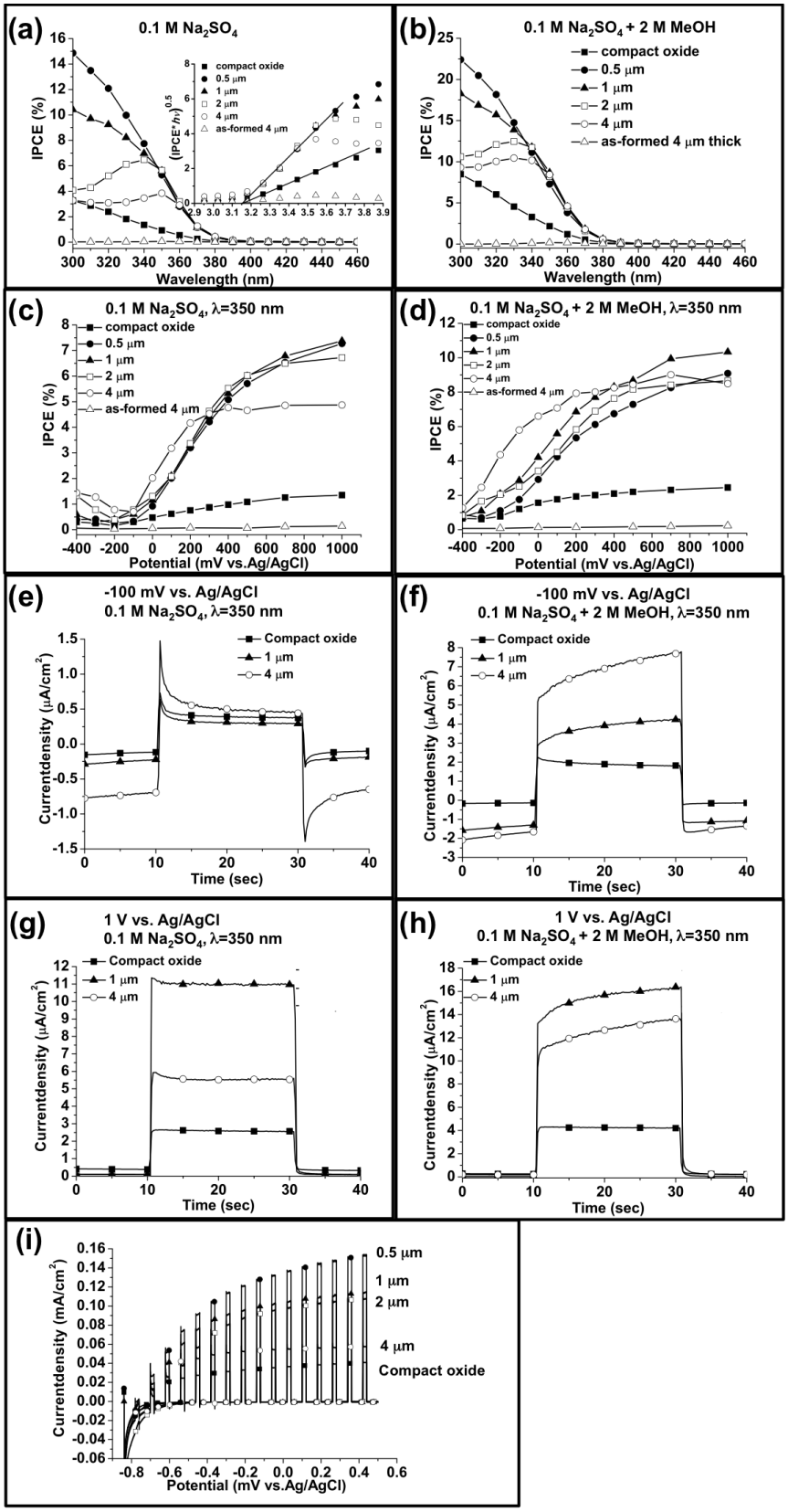
(a)
0.1 M Na2SO4
IPCE (%)
Wavelength (nm)
compact oxide
0.5 μm
1 μm
2 μm
4 μm
as-formed 4 μm
(IPCE*hν)^0.5
(b)
0.1 M Na2SO4 + 2 M MeOH
IPCE (%)
Wavelength (nm)
compact oxide
0.5 μm
1 μm
2 μm
4 μm
as-formed 4 μm thick
(c)
0.1 M Na2SO4, λ=350 nm
IPCE (%)
Potential (mV vs.Ag/AgCl)
compact oxide
0.5 μm
1 μm
2 μm
4 μm
as-formed 4 μm
(d)
0.1 M Na2SO4 + 2 M MeOH, λ=350 nm
IPCE (%)
Potential (mV vs.Ag/AgCl)
compact oxide
0.5 μm
1 μm
2 μm
4 μm
as-formed 4 μm
(e)
-100 mV vs. Ag/AgCl
0.1 M Na2SO4, λ=350 nm
Currentdensity (μA/cm2)
Time (sec)
Compact oxide
1 μm
4 μm
(f)
-100 mV vs. Ag/AgCl
0.1 M Na2SO4 + 2 M MeOH, λ=350 nm
Currentdensity (μA/cm2)
Time (sec)
Compact oxide
1 μm
4 μm
(g)
1 V vs. Ag/AgCl
0.1 M Na2SO4, λ=350 nm
Currentdensity (μA/cm2)
Time (sec)
Compact oxide
1 μm
4 μm
(h)
1 V vs. Ag/AgCl
0.1 M Na2SO4 + 2 M MeOH, λ=350 nm
Currentdensity (μA/cm2)
Time (sec)
Compact oxide
1 μm
4 μm
(i)
Currentdensity (mA/cm2)
Potential (mV vs.Ag/AgCl)
0.5 μm
1 μm
2 μm
4 μm
Compact oxide